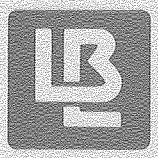

Lawrence Berkeley Laboratory
UNIVERSITY OF CALIFORNIA

Materials & Molecular Research Division

To be published in Analytical Chemistry

SEPARATION OF OVERLAPPED ELECTROCHEMICAL PEAKS USING THE KALMAN FILTER

Teri F. Brown and Steven D. Brown

January 1981

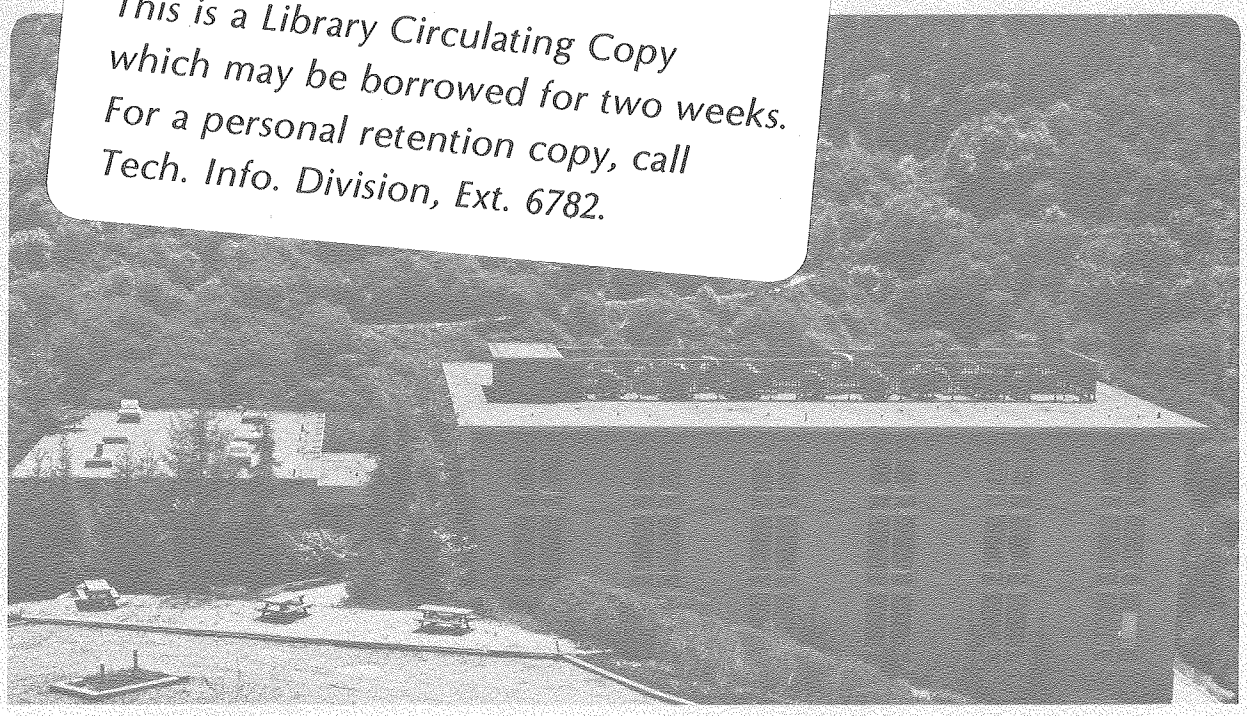

Prepared for the U.S. Department of Energy under Contract W-7405-ENG-48

DISCLAIMER

LBL-11917

Separation of Overlapped Electrochemical Peaks Using the Kalman Filter

by

Teri F. Brown, Department of Civil Engineering, University of Washington, Seattle, WA 98195 and Materials and Molecular Research Division, Lawrence Berkeley Laboratory, Berkeley, CA 94720

and

Steven D. Brown*, Department of Chemistry, University of California, Berkeley, CA 94720 and Materials and Molecular Research Division, Lawrence Berkeley Laboratory, Berkeley, CA 94720

Submitted to Analytical Chemistry

January 15, 1981

This work was supported by the Director, Office of Energy Research, Office of Basic Energy Sciences, Chemical Sciences Division of the U.S. Department of Energy under Contract No. W-7405-ENG-48.

Brief

Quantitative resolution of peaks generated by linear scan voltammetry is possible, even when peaks are separated by as little as 2.5 mv. Noise and background are also removed by the filter.

Separation of Overlapped Electrochemical Peaks Using the Kalman Filter

Teri F. Brown, Dept. of Civil Engineering, University of Washington, Seattle WA 98195 and Materials and Molecular Research Division, Lawrence Berkeley Laboratory, Berkeley, CA 94720 and
Steven D. Brown*, Dept. of Chemistry, University of California at Berkeley and Materials and Molecular Research Division, Lawrence Berkeley Laboratory, Berkeley, CA 94720

Abstract

A major limitation in the use of electrochemical techniques for the quantitative analysis of mixtures is the difficulty of resolving overlapped peaks. This problem is further complicated by the low signal-to-noise ratios often encountered in trace analysis and by the use of electrochemical techniques that produce broad, asymmetric waveforms. This paper demonstrates the use of the Kalman Filter for multi-component analysis of linear sweep voltammograms. Even with the broad, asymmetric LSV waveform, synthetic data runs show that a peak separation of as little as 2.5 mV is sufficient for peak deconvolution in the presence of random noise. Besides separating overlapped peaks, the methods also filters the noise from the signal and can be used to separate the capacitive current component from the faradaic current component. The method is validated further using the Cd(II)/In(III) and Cd(II)/In(III)/Pb(II) systems which show peak separations of 40 to 200 mV. The use of the techniques with two other voltammetric waveforms is also demonstrated.

INTRODUCTION

Electrochemical techniques show great promise for the analysis of complex mixtures because of their ability to determine both concentrations and stability constants. Unfortunately, the methods are limited by the difficulty of resolving overlapped peaks. This is especially true in trace analysis where the signal-to-noise ratio may be low. Recent techniques have been able to separate peaks which are similar in height and have half-wave potentials as close as 30 to 40 mV using either semiderivative voltammetry (1) or square wave voltammetry (2) combined with modern data analysis techniques.

Three approaches have been used for the deconvolution of overlapped electrochemical peaks. The first approach fits the data to a previously defined functional shape such as the $sech^2$ function used in convolution voltammetry (1) or the empirical functions used by Perone in stationary electrode polarography (3) or in square wave voltammetry (2). In this method, the peak shape of each component is defined by the general functional shape and 3 to 9 parameters. This procedure may be used to reduce the noise in a single component system, or to separate peaks and reduce noise in a multi-component system. Besides the general problem of choosing the correct functional shape, there are three important limitations to the method: 1) the correct number of components must be specified, 2) the peaks must be separated enough to be distinguishable (this is usually expressed as a minimum separation per unit width of the wider peak), and 3) the computational load is heavy, i.e., to fit a four parameter system would require the iterative determination of 12 to 36 parameters point by point along the voltammogram.

The second approach, which is less mathematical in nature, uses a micro-

processor controlled polarograph to subtract a background solution from the multi-component solution (4). Aliquots of all but one of the components are added into the background solution and the polarographic measurement is repeated until visual inspection of the difference polarogram shows the complete removal of all but one peak. The height of the remaining peak is related to its concentration via a standardization curve. This process is repeated for each component in the mixture. Not only is this method extremely time consuming, but the background subtraction increases the noise in the difference polarogram from which the peak height is determined.

The last approach uses linear parameter estimation to determine the concentration of each component in a mixture and is exemplified by Binkley and Dessy (5) working with square wave voltammetry (SWV). This method uses single component SW voltammograms which have been normalized by dividing by their concentration to define the line shapes and positions of the components. A linear model is assumed in which the products of each component's concentration times its line shape are added to yield the mixture voltammogram. The individual concentrations are treated as unknown parameters and are determined through a batch minimization process. Binkley and Dessy performed the linear parameter estimation in the Fourier frequency domain instead of in the time domain because this greatly reduced the size of the matrices used in the algorithm. This reduction in dimensionality occurs because the low frequency components of the Fourier domain contain the information needed to deconvolute the peaks; the high frequency components are mostly noise.

The peak separation technique presented in this paper uses the Kalman filter, a recursive digital filtering algorithm, for linear parameter estimation of multi-component voltammetry data in the time domain. The mathematical formulation of the Kalman Filter eliminates the problem of manipulating large

matrices; this makes it possible to perform time domain calculations rapidly on small laboratory computers. Additionally, the algorithm yields not only optimal estimates of the variables, but also their covariance matrix. In data with noise, this covariance matrix estimate is necessary to determine the error in the estimate. A discussion of the notation used in linear parameter estimation theory and three simple chemical examples can be found in a recent review of the subject (6).

THEORY

The Kalman Filter is a specific algorithm derived by Kalman in the early 1960's (7,8,9), which can be used for linear parameter estimation. Its application requires more stringent assumptions about the structure of the electrochemical noise than do the other least squares algorithms (6,8), but if these assumptions are met the Kalman Filter estimate is the optimal estimate, in either the least squares or the maximum likelihood sense, of both the system parameters and their covariance matrix (10). Additionally, the algorithm is fast, easy to program, and, because it is recursive, does not require much computer memory.

Application of the Kalman Filter requires formulation of the problem in state-space notation. The general approach requires the specification of 1) a model of the system dynamics, 2) a measurement function that relates the measureables of the system (such as current or potential) to the state variables of the system (such as concentration), and 3) initial guesses of the variables. Table I. is a summary of the Kalman Filter equations for the discrete time case. The system model equation defines how the system would evolve in time. Its first term is a model of the system dynamics; the second

term represents random fluctuations in the model. The measurement function also has two terms: the first to define the relationship between measureables and state variables, and the second to handle the noise present in the measurements. Since the algorithm is not self-starting, it is necessary to specify initial guesses of the state variables, although for a statistically robust system the final estimate of the state variables should be very nearly independent of the initial guess. The next three equations in Table I. are the noise assumptions; they state that the noise contained in the system model and in the measurements must be defined by noise processes with mean values of zero, with known variances, and which are uncorrelated with each other in time. In simpler words, the equations require that the noise be from independent, white noise processes.

The next five equations in Table I. are the equations of the actual Kalman Filter algorithm. The first two equations are calculated prior to each measurement; they determine the optimal estimate of the state vector, $\underline{X}$ and its covariance matrix, $\underline{\underline{P}}$, based on the system dynamics alone. The next three equations add the information contained in the measurement, $\underline{Z}$, to form the optimal estimates of $\underline{X}$ and $\underline{\underline{P}}$ based on both the system dynamics and the latest measurement.

The Kalman Filter contains one last criterion that must be met -- observability. This verifies that there is enough information contained in the measurement vector, $\underline{Z}$, so that it is possible to determine the state vector, $\underline{X}$. Mathematically, this involves showing that the observability matrix, $\underline{\underline{\chi}}$, is of rank n, where n is the number of state variables. $\underline{\underline{\chi}}$ is defined as:

$$\underline{\underline{\chi}}(t) = \left[\underline{\underline{S}}^T \;\vdots\; \underline{\underline{H}}^T \cdot \underline{\underline{S}}^T \;\vdots\; \underline{\underline{H}}^T \cdot \underline{\underline{H}}^T \cdot \underline{\underline{S}}^T \;\vdots\; \cdots \;\vdots\; (\underline{\underline{H}}^T)^{n-1} \cdot \underline{\underline{S}}^T \right] \qquad \text{(eqn. 1)}$$

Rigorous application of this equation is tricky. However, a conceptually simple example of when the criteria would fail is if the value of $\underline{S}(t)$ for two different components is the same for all time. When this is so, the two components are not linearly independent and $\underline{\underline{X}}(t)$ will be singular.

The Kalman Filter was formulated originally with time as the independent variable; a formulation that still permeates the literature. However, any other independent variable is acceptible as long as the noise assumptions can be met in terms of that variable. For electrochemical techniques using linear scan mechanisms to scan potential, the transformation is simple because the new independent variable, potential, is linear with time.

For the example of a voltammogram with overlapped peaks, the state vector consists of the concentration (or peak height) of each component, and the independent variable is potential. The system model equation has the identity matrix as the state transition matrix because the bulk concentration of each component is constant throughout the run. The measurement function model is given by:

$$Z(E) = S_1(E) \cdot X_1 + S_2(E) \cdot X_2 + \cdots + S_N(E) \cdot X_N + \nu(E) \qquad \text{(eqn. 2)}$$

or, in state-space notation:

$$Z(E) = \underline{S}^T(E) \cdot \underline{X} + \nu(E) \qquad \text{(eqn. 3)}$$

where $Z(E)$ is the value of the current at potential E, $\nu(E)$ is the noise in the measurement of the current, $\underline{X}$ is the column vector of the concentrations of each component, and $\underline{S}^T$ is the row vector defining the measurement function. The Kalman Filter equations for this example are given in Table II. Because there is only one measureable quantity, current, the dimensionality of the problem is greatly reduced. The only matrix that remains is the symmetric covariance matrix, and the matrix inversion required for the filter gain matrix (which is now reduced to a vector) determination has been reduced to

a scalar divide. Additionally, the system model is assumed to be noise free. This will cause the state covariance matrix to be slightly underestimated by the filter, as can be seen by comparing the covariance matrix extrapolation equations in Tables I. and II.

The measurement function, $\underline{S}(E)$, is calculated from the single component voltammograms that have been normalized by dividing by their concentrations. Figure 1. shows a sample input for a two component system; here, Y1(E) is a single component scan of 8.36×10^{-5}M Cd(II), Y2(E) is a single component scan of 8.09×10^{-5} M In(III), and Z(E) is an unknown mixture of Cd(II) and In(III). The measurement function for this example would be calculated as:

$$S(E) = \begin{bmatrix} Y1(E)/8.09\times10^{-5} \\ Y2(E)/8.36\times10^{-5} \end{bmatrix} \qquad \text{(eqn. 4)}$$

There is noise in the single component scans, Y1(E) and Y2(E); yet, the Kalman Filter derivation assumes that the measurement function is known exactly. For the case where the measurement function does contain noise, the measurement model would be better described by:

$$Z(E) = S^{T}(E)\cdot X + F^{T}(E)\cdot\omega(E) + \nu(E) \qquad \text{(eqn. 5)}$$

where $\omega(E)$ is the vector of random noise of $\underline{S}(E)$, and $\underline{F}^{T}(E)$ is the vector of weights for the measurement function noise components. Although it is possible to determine the covariance matrix of $\omega(E)$ from the variance of the noise in the single component voltammograms, it is very difficult to determine the form of the $\underline{F}(E)$ vector. For this reason, $\underline{F}(E)$ is assumed to be the identity vector which has the effect of assuming equal weights. Additionally, it is necessary for the noise processes in the single component data to be independent, white noise processes. With these assumptions, the measurement function model equation can be rewritten as:

$$Z(E) = S^{T}(E)\cdot X + \omega_1(E) + \omega_2(E) + \cdots + \omega_N(E) + \nu(E) \qquad \text{(eqn. 6)}$$

or if the random variables are added together to get an effective noise component, $\nu'(E)$, as in:

$$Z(E) = S^T(E) \cdot X + \nu'(E) \qquad \text{(eqn. 7)}$$

For independent noise processes, the variance of the sum is the sum of the variances of the components. The variance of a voltammogram at each point can be found by averaging many replicate voltammograms; this is a long and tedious process. Fortunately, we found that the magnitude of the variance was independent of the potential and that it could be estimated from the high frequency componentsof the Fourier power spectrum (11).

Poulisse (12,13,14) has used a similar formulation of the Kalman Filter to separate the overlapped ultra-violet spectra of organic compounds. His work used a different formulation of the effective variance of the spectra, in part, because of the problem of determining the variance of a UV spectra. Additionally, he proposes using the Kalman Filter for on-line drift compensation (14). This same approach could be used to remove the capacitive current component in LSV in those cases where it is approximately linear over the scan. Instead, we chose to treat the capacitive current as though it were another peak and used the background scan to generate the necessary term in the measurement function. This process avoided the assumption of linear capacitive current.

EXPERIMENTAL

Reagents: Stock solutions of approximately 1.0×10^{-2}M Pb(II) and Cd(II) were made by dissolving A.R. grade metallic lead and cadmium, respectively, in A.R. grade nitric acid and then diluting with quartz distilled water. The In(III) solution was made in an analogous manner from 99.95% In_2O_3 dissolved in a minimum amount of hot 72% $HClO_4$. Aliquots of these solutions were titrated with a standard EDTA solution, and the following stock concentrations were

determined: [Pb(II)] = 1.96×10^{-2} M; [Cd(II)] = 2.09×10^{-2} M; and [In(III)] = 2.02×10^{-2}M. All solutions were made 0.58 M in A.R. grade HCl, which had been further purified by subboiling distillation in a Teflon still (15).

Cells, electrodes, and equipment: The cell used for all runs was the standard Princeton Applied Research (PAR) polarographic cell and cell holder, thermostated to 24.9±0.1 C. The working electrode was a PAR 9323 HMDE. The reference electrode was a Ag/AgCl electrode with a 1.0 M $NaClO_4$/0.1 M NaCl salt bridge; its potential was +40 mV vs. SCE. The counter electrode was a length of heavy gauge platinum wire. All solutions were degassed using purified Argon gas to remove oxygen. A PAR 173 potentiostat was used to apply potentials to the cell. The scans were controlled with either a PAR 175 ramp generator or a 16-bit digital-to-analog (D/A) converter optically coupled to the parallel interface provided on the computer. A Digital Equipment Corporation MINC-11B computer, equipped with a 12-bit A/D converter, four 12-bit D/A converters, a programmable real time clock, parallel I/O interface, and serial I/O interface was used to control the experiment and collect the data. The CPU was an LSI 11/2 unit with 30K words of usable memory.

Control of the LSV experiment was performed by MACRO-11 assembly language routines linked with a FORTRAN driver and other MACRO and FORTRAN subroutines for graphics and data storage; all running under the RT-11 monitor. The data was stored on floppy disc for later processing on a separate LSI-11/23 CPU. Data processing included noise reduction using fast Fourier filtering techniques (16) and background subtraction to remove the capacitive current component (17). Semidifferentiation to produce semiderivative voltammograms (SDV) (18) and semiintegration to yield neopolarograms (19) was available using the GI algorithm based on Grunwald's definition of differintegration (20). All programs except the fast Fourier transform (FFT) subroutine were

written by our group; the FFT subroutine, based on the Cooley-Tukey algorithm, was obtained from the Digital Equipment Corporation Laboratory Applications-11 Software package. Data processing, without differintegration, took less than 1 minute per file.

Laboratory procedure: Six series of LSV standard addition experiments were performed; they were:

1) standard additions of Cd(II) to supporting electrolyte solution,
2) standard additions of In(III) to supporting electrolyte solution,
3) standard additions of Pb(II) to supporting electrolyte solution,
4) standard additions of Cd(II) to supporting electrolyte solution which was $5.88 \times 10^{-}$ M in In(III),
5) standard additions of In(III) to supporting electrolyte solution which was 8.36×10^{-5} M in Cd(II), and
6) standard additions of Cd(II) to supporting electrolyte solution which was 8.09×10^{-5}M in In(III) and 7.86×10^{-5}M in Pb(II).

The additions were made from the stock solutions using Eppendorf pipettes. After degassing each solution with purified Argon, a potential of -0.200 V vs Ag/AgCl reference electrode was applied to the cell. The potential was then scanned using a linear ramp to -0.900 V; the scan rate was 1 volt per second and 512 uniformly spaced points were taken and stored on disc. Standardization curves were made from the three runs of single component data; the three linear least squares fits gave correlation coefficient values of 0.9998, 0.9996, and 0.9988, respectively.

Synthetic data generation: Synthetic LSV data was generated from tabulated values of the X(at) function described by Nicholson and Shain (21) for reversible systems. Given the X(at) function, the half-wave potential ($E_{1/2}$),

the number of electrons (n), and the concentration (C), synthetic voltammograms were constructed by a FORTRAN program using:

$$i(E) = \beta \cdot C \cdot n \cdot \chi(E - E_{1/2}) \qquad \text{(eqn. 8)}$$

where b was a constant which included the scan rate, the temperature, and the diffusion coefficient. Single component voltammograms were added together point by point to produce multi-component voltammograms. Additionally, white noise constructed from a Gaussian random number generator could be added by specifying the desired signal-to-noise (S/N) ratio. Synthetic semiderivative voltammograms were constructed to test the effect of lineshape on the Kalman Filter and to determine the value of semidifferentiation of the data. The SD voltammograms were constructed in a manner similar to the LS voltammograms, except that the defining equation for the semiderivative wave was given by:

$$e(E) = \gamma \cdot n \cdot C \cdot \mathrm{sech}^2 \{ n \cdot f \cdot (E - E_{1/2}) \} \qquad \text{(eqn. 9)}$$

where f = F/2RT and g includes the scan rate, the temperature, and the diffusion coefficient.

Peak separation procedure: Peak separation was performed using a FORTRAN program, KFMCA, which was based on the Kalman Filter algorithm, but which was written specifically to perform peak deconvolution rapidly. The program first calculated the measurement function from the single component voltammograms and their concentration (or peak heights). Next the multi-component voltammogram data file was read in and the effective variance calculated as the sum if its variance and the variances of the single component voltammograms. Lastly, initial guesses of the concentration and the variance of each component were needed to start the algorithm. Although either concentration or peak height could be used as the state variable, it was important to choose a unit system such that most of the values fell between 10^{-2} and 10^{+2} in order to avoid computer round-off error. In this paper, peak heights in μamps were

used. The program output consisted of the optimal estimates of the concentrations of each component and their covariance matrix; additionally, four measures of overall goodness of fit were calculated - the variance of the fit, the average relative error, the squared correlation coefficient, and the coefficient of determination (22). The coefficient of determination is given by:

$$CD = 1.0 - \frac{\sum_{i=1}^{N} (Y_i - Y(X_i))^2}{\sum_{i=1}^{N} Y_i^2} \qquad \text{(eqn. 10)}$$

where Y_i is the experimental curve, $Y(X_i)$ is the fit curve, and N is the number of data points. For best results the single component voltammograms should be Fourier filtered and background subtracted; this process is helpful but not necessary for the multi-component data. Since the final estimate was found to depend slightly on the initial guess, the program was allowed to iterate up to 5 times through the data points, using the final extimate as the initial guess on the next iteration. This whole procedure is pictured in figure 2.

RESULTS AND DISCUSSION

The peak separation technique was tested using synthetic LSV data, synthetic SDV data, and real LSV data from two component Cd(II) and In(III) systems and from a three component Cd(II)/In(III)/Pb(II) system. The method is applicable to a width range of waveforms, but the broad asymmetric LSV waveform and the narrow, symmetric SDV waveform represents extremes of those typically encountered in electrochemistry. Additionally, a brief application of the method to neopolarographic waves (19) was demonstrated. Four measures

of the overall fit were tried: the variance of the fit, the average relative error, the squared correlation coefficient, and the coefficient of determination. The squared correlation coefficient was very close in value to the coefficient of determination (CD), but was tedious to calculate and contained large round-off errors. The average relative error, even with a modified denominator, tended to blow up to unrealistic values. The variance of the fit and the CD were useful measures of different aspects of the fit. The CD was independent of the properties of the system being fit and allowed for rapid comparison of widely different systems. However, the variance of the fit was much more sensitive to changes in parameters, in the structure of the model, and in the measurements, but less sensitive to round-off errors. However, its magnitude depends on both the magnitude of the signal and on the signal-to-noise ratio; this limits its use for intersystem comparisons. Perone (2,3) also recommends using these two values as measures of the goodness of fit. For systems with moderate amounts of noise, the variance of the fit was found to be much larger than the variance elements of the estimated concentrations; this was a good indication of the successful removal of the random noise and showed the importance of calculating the covariance matrix.

The synthetic data were used to determine the sensitivity of the method to different peak shapes, to differences in peak height and position, to the S/N of the data, and to errors in the input parameters or in the model. The results and a few examples are given below:

1. Effect of Peak Shape. In general, better results were obtained with the LSV data than with the SDV data, even for the same systems. This effect is shown in Table III.; the terms of the covariance matrix and the percent error in the components were smaller for the LSV data than for the SDV data. The variances of the fit do not show this effect as

clearly because the magnitude of the LSV signal is larger than the the SDV signal. This preference for the LSV data is in direct contrast to most other fitting techniques which prefer narrow, symmetric peaks because of decreased peak overlap and fitting parameters. However, asymmetric peaks contain more information than their symmetric analogs, i.e., more moments are necessary to describe them. Because our technique stores all lineshape information in the measurement function, this extra information does not increase the number of parameters nor the computational load and, therefore, is effectively free. Figure 3. shows a comparison of the separation of a two component system using LSV data and SDV data. In general, the fits of the SD voltammograms gave errors that were 1-100% larger than the LSV fits.

2. Effect of Peak Separation. To determine the minimum difference in peak potential of the two peaks which allowed for a quantitative resolution of the two peaks, a series of runs were made with two equal height peaks separated by 50, 25, 10, 5, and 2.5 mV. The minimum difference was found to depend on the point density of the scans, i.e., on the number of observations per unit of the potential scan. For 512 point scans over a 0.50 V range, a 2.5 mV separation of the peak potentials was sufficient to give fits with less than 0.1% error in the estimated peak heights. When the peaks were of unequal heights, the error in the smaller peak was seen to increase; but for peaks with height ratios of 1 to 10, quantitative resolution was still possible at 2.5 mV peak separation. Table IV. summarizies these results. The 2.5 mV separation is a factor of 10 improvement over reported values using other techniques, and could be further decreased by increasing

the point density in the critical range. This improvement is not possible with most other techniques, since they do not depend on the point density. Improvement might be possible with the technique of Binkley and Dessy (5), if the increased point density has the effect of increasing the information in the imaginary component in Fourier space.

3. Effect of Errors in Peak Position. With the ability to separate fused peaks with peak potentials as close as 2.5 mV, the problem of peak shifts between the single component voltammograms used to generate the measurement function and the multi-component voltammogram became appreciable. This shift may be caused by an inability to match the backgrounds, by ligand concentration effects, or by unknown synergistic effects in the mixture. An initial study to estimate the magnitude of this problem showed that a shift of 7.5 mV in the mixture voltammogram from its original position was sufficient to increase the errors in the estimated concentrations to greater than 50% for peaks within 30 mV of each other. In an attempt to circumvent this problem, a synthetic voltammogram of a two component system which contained two peaks with half-wave potentials of -0.500 and -0.550 V was examined. The single component voltammogram for component two has a peak at -0.550 V; but for component one a series of single component voltammograms were tried with peak potentials from -0.490 V to -0.510 V. The results are presented in Table V. Note the very sharp decrease in the variance of the fit when the correct half-wave potential was found. This behavior was seen in noise corrupted scans, also. The sensitivity of the variance to the peak potential position allowed for a determination of a probable shift and an accurate measurement of its magnitude.

4. Effect of Errors in the Initial Guess. The next study dealt with the detection of one peak in between two large peaks with various initial guesses. Table VI. shows the results of four runs in which the three peaks were separated by 25 mV from each other and had peak height ratios of 1:1:1 or $1:^{1}/_{10}:1$. As expected, the worst case was with a small middle peak and low S/N. However, even in this case, and with an initial guess of the presence of only the two larger components, the filter algorithm was able to separate the peaks and estimate the peak heights of the two outside peaks to within 5%. The percent error in the estimate of the height of the middle peak was greatly reduced when the accuracy of the initial guess was improved. This study presented a worst case situation; for less overlapped systems, the initial guess could be incorrect by a factor of 10 to 100 without effecting the value of the final estimate. Strangely, for very strongly overlapped systems, extremely poor initial guesses were sometimes found to cause more rapid convergence to the correct value.

5. Effect of Peak Width and Changes in Peak Width. The effect of peak width on the minimum difference in peak potential for quantitative resolution was minimal up to a peak width of 60-70 mV. At peak widths of greater than 90 mV the minimum separation was nearer to 5.0 mV. The effect was stronger, the lower the S/N of the voltammogram. A more critical effect occurred when the peak width changed between the single component voltammogram and the multi-component voltammogram. This study was done with synthetic SDV data because of the difficulty of modifying the LSV data to peak widths cooresponding to non-integral

electron transfer or irreversible reactions; the results with LSV data would be expected to give slightly lower errors. Table VII. shows the results from a series of runs where either peak broadeding or narrowing occurred between the single component and multi-component runs. These runs were chosen to represent a worst case, because the peaks are only separated by 10 mV and the peak height ratio is 1 to 10 with the larger peak going through the peak width changes. When the large peak was broadened, the error in the small peak was very large because the filter was unable to attribute the large increase in overlap to the large peak and attempted to assign it to the smaller.

Since the synthetic data runs showed that the LSV data with high S/N gave the best results, the real data was Fourier filtered and background subtracted before peak separation, but not semidifferentiated nor semiintegrated. The actual procedure of peak separation and estimation of component concentrations consisted of four steps:

1. making standard addition curves from the single peak data for each component,
2. using the highest concentration run from the standard addition curve as the single component voltammogram to form the measurement function,
3. running the filter to estimate the peak height, and
4. using the peak heights and the standard addition curves to determine the concentration.

Visual inspection of the results, as in figure 4, showed that small peak shifts were occurring between the single and multi-component voltammograms. This shift increased the variance of the fit, the percent error in each component, and the covariance matrix of the estimated peak heights. Additionally, it caused the innovations sequence of the Kalman Filter to be correlated;

an indication of nonoptimal performance by the Kalman Filter (10). This can be seen in figure 4 by looking at the residuals of the fit which is related to the innovation sequence. The KFMCA program was modified to allow for shifts of ±5 mV about the single component value, in increments of about 1.2 mV. The variance of the fit was used to determine an improved fit. Figure 5 shows the reults using the modified program on the same system shown in figure 4. Note that the residuals of the fit (or the innovation sequence) looks much flatter and less correlated. Table VIII. is a summary of the results for the two component systems of Cd(II) and In(III). The coefficient of determination was better than 0.9995 for all fits. The percent error in the estimated concentration included errors caused by experimental technique, changes in the standard addition curve, and by the fitting algorithm. Table IX. presents the results for the three component Cd(II)/In(III)/Pb(II) system. Again, the filter gave quantitative resolution of the peaks, accurate estimates of the concentrations, and estimates of the peak shifts in the mixture.

As a final comparison, figure 6 shows the results of the fits of a two component Cd(II)/In(III) voltammogram using four different procedures:

1. multi-component data file was left unmodified; single component data files were Fourier filtered and background subtracted; and a scan of the background was used to model the capacitive current prior to peak separation,
2. all data files were Fourier filtered and background subtracted prior to peak separation,
3. all data files were Fourier filtered, background subtracted, and semidifferentiated prior to peak separation, and
4. all data files were Fourier filtered, background subtracted, and semiintegrated prior to peak separation.

In all four procedures quantitative resolution of the peaks was possible. Procedure one (figure 6A) used the Kalman Filter to separate the current response into a capacitive current component, and two faradaic current components, and noise which is contained in the innovation sequence. Procedure two (figure 6B) shows the effect of background subtraction and Fourier filtering prior to peak separation; the capacitive current component is gone and the slight structure in the innovation sequence is caused by small errors in the model and by low frequency noise. (In our case, it was mostly low frequency noise from a particle accelerator in the next building.) Procedures 3 and 4 were used to demonstrate the versatility of the Kalman Filter for a variety of waveforms.

ACKNOWLEDGMENT

The authors would like to thank another member of our group, Jeff Toman, would allowing us to use his Cd(II)/In(III)/Pb(II) data in our paper.

Credit

This work was supported by the Director, Office of Energy Research, Office of Basic Energy Sciences, Chemical Sciences Division of the U.S. Department of Energy under Contract No. W-7405-ENG-48.

REFERENCES:

(1) Toman, J.J.;Brown, S.D. submitted for publication in Anal. Chem.

(2) Boudreau, P.A.;Perone, S.P. Anal. Chem. 1979,51,811-817.

(3) Gutknecht,W.F.;Perone, S.P. Anal. Chem. 1970,42,906-917.

(4) Bond, A.M.;Grabaric, B.S. Anal. Chem. 1976,48,1624-1628.

(5) Binkley, D.P.;Dessy, R.E. Anal. Chem. 1980,52,1335-1344.

(6) Brubaker, D.P.,Tracy, R.;Pomernacki, C.L. Anal. Chem. 1978,50,1017A.

(7) Kalman, R.E. Trans. ASME, Ser. D, J of Basic Eng. 1960,82,34-45.

(8) Kalman, R.E.;Bucy, R.S. Trans. ASME, Ser. D, J of Basic Eng. 1961, 83,95-107.

(9) Kalman, R.E. "New Methods in Weiner Filtering Theory", Proceedings of the First Symposium on Engineering Applications of Random Function Theory and Probabilty, J.L. Bagdanoff and F. Kozin (eds.), Wiley: New York, 1963;270-388.

(10) Gelb. A. (ed.) "Applied Optimal Estimation"; M.I.T. Press: Cambridge, Mass., 1974; Chapter 4.

(11) Brown, T.F.;Brown, S.D. paper 184, Pittsburgh Conference on Analytical Chemistry and Applied Spectroscopy 1981.

(12) Poulisse, H.N.J. Anal. Chim. Acta 1979,112,361-374.

(13) Didden, C.B.M.;Poulisse, H.N.J. Anal. Letters 1980,13(A11),921-935.

(14) Poulisse, H.N.J.;Engelen, P. Anal. Letters 1980,13(A14),1211-1234.

(15) Mattison, J.M. Anal. Chem. 1972,44,1715-1716.

(16) Hayes, J.W.;Glover, D.E.;Smith, D.E.;Overton, M.W. Anal. Chem. 1973, 45,277.

(17) Brown, S.D;Kowalski, B.R. Anal. Chim. Acta 1979,107,13-27.

(18) Goto, M.;Ishii, D.J. J. of Electroanal. Chem. 1975,61,361-365.

(19) Grenness, M.;Oldham, K.B. Anal. Chem. 1972,44,1121-1129.

(20) Oldham, K.B.;Spanier, J. "Fractional Calculus" (Vol.111 in Math. in Science and Eng, Series); Academic Press: New York, 1974; Chapter 8.

(21) Nicholson, R.S.;Shain, I. Anal. Chem. 1964,36,706-723.

(22) Mosteller, F.;Tukey, J.W. "Data Analysis and Regression"; Addison Wesley: Reading, Mass., 1977.

Figure Captions

Figure 1. Input Voltammograms: Y1(E) is the single component Cd(II) voltammogram; Y2(E) is the single component In(III) voltammogram; and Z(E) is an unknown mixture of Cd(II) and In(III).

Figure 2. Flow chart for peak separation using the Kalman Filter.

Figure 3. Comparison of synthetic LSV and SDV data. Both systems are two component systems with a peak potential separation of 25 mV and peak height ration of 1:1/10. All charge transfer reactions are 1 electron reactions. S/N = 40.0 for the LSV data and 20.0 for the SDV data because semidifferentiation doubles the magnitude of the noise.

Figure 4. Peak separation of a two component Cd(II)/In(III) system: I. Cd(II) wave, II. In(III) wave, III. Sum of Cd(II) and In(III) waves, IV. The original voltammogram, and V. The residuals of the fit (also, called the innovation sequence). Note the poor fit and the distinctive sinusoidal pattern in the residuals. This is an indication of peak shift between the single component and the multi-component voltammograms.

Figure 5. Peak separation of the same Cd(II)/In(III) as shown in Figure 4 using the modified KFMCA routine. The Cd(II) and In(III) waves were found to have shifted 3 mV between the single component and multi-component scans. Note the greatly improved fit and the almost flat residual curve.

Figure 6. Demonstration of the peak separation for a two component Cd(II)/In(III) system using four different procedures: A. Raw data with capacitive current treated as a third component;

B. Prefiltered data; C. Prefiltered and semidifferentiated data; and D. Prefiltered and semiintegrated data. Each graph contains plots of the original voltammogram, the separated component voltammograms and their sum and the residuals of the fit.

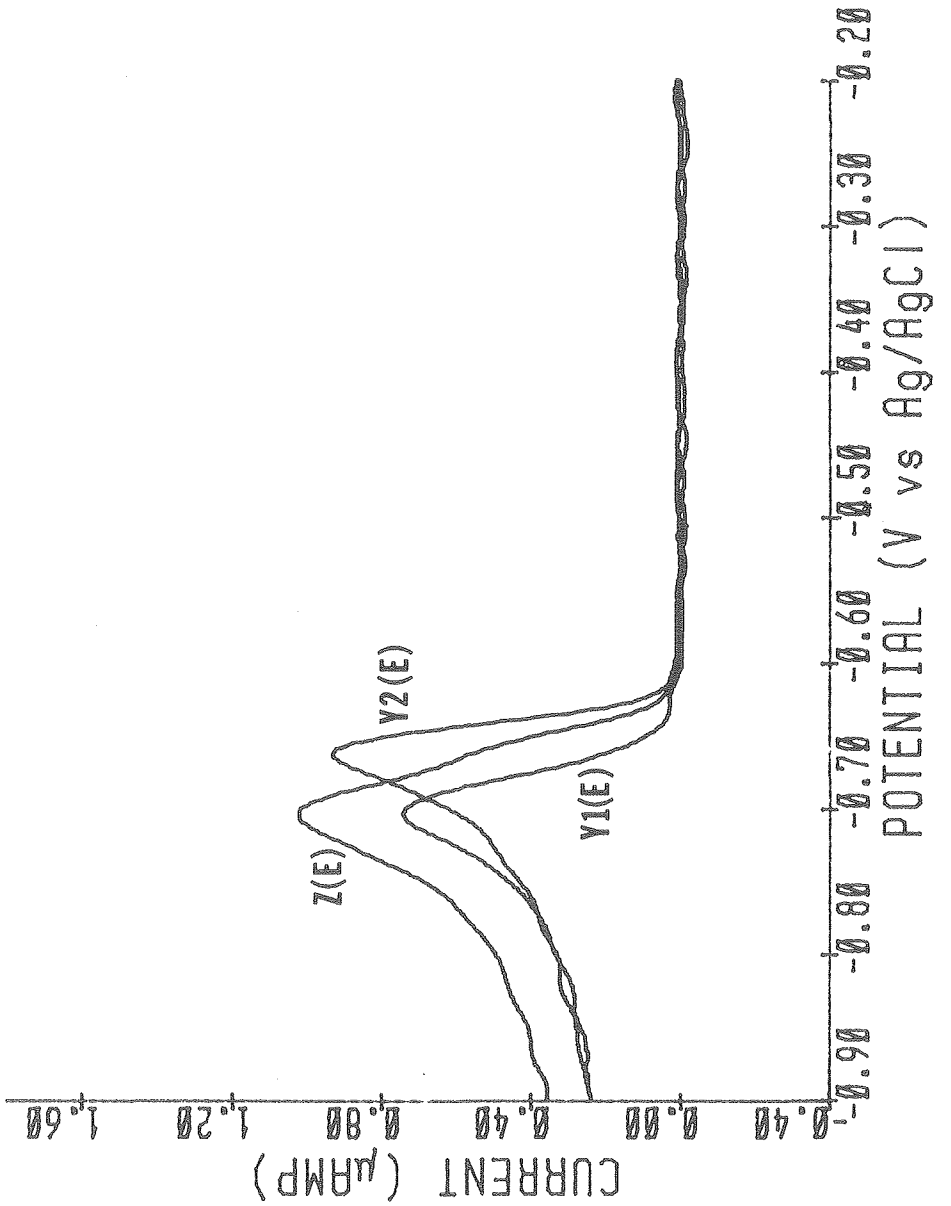

XBL 811-7549

Figure 1.

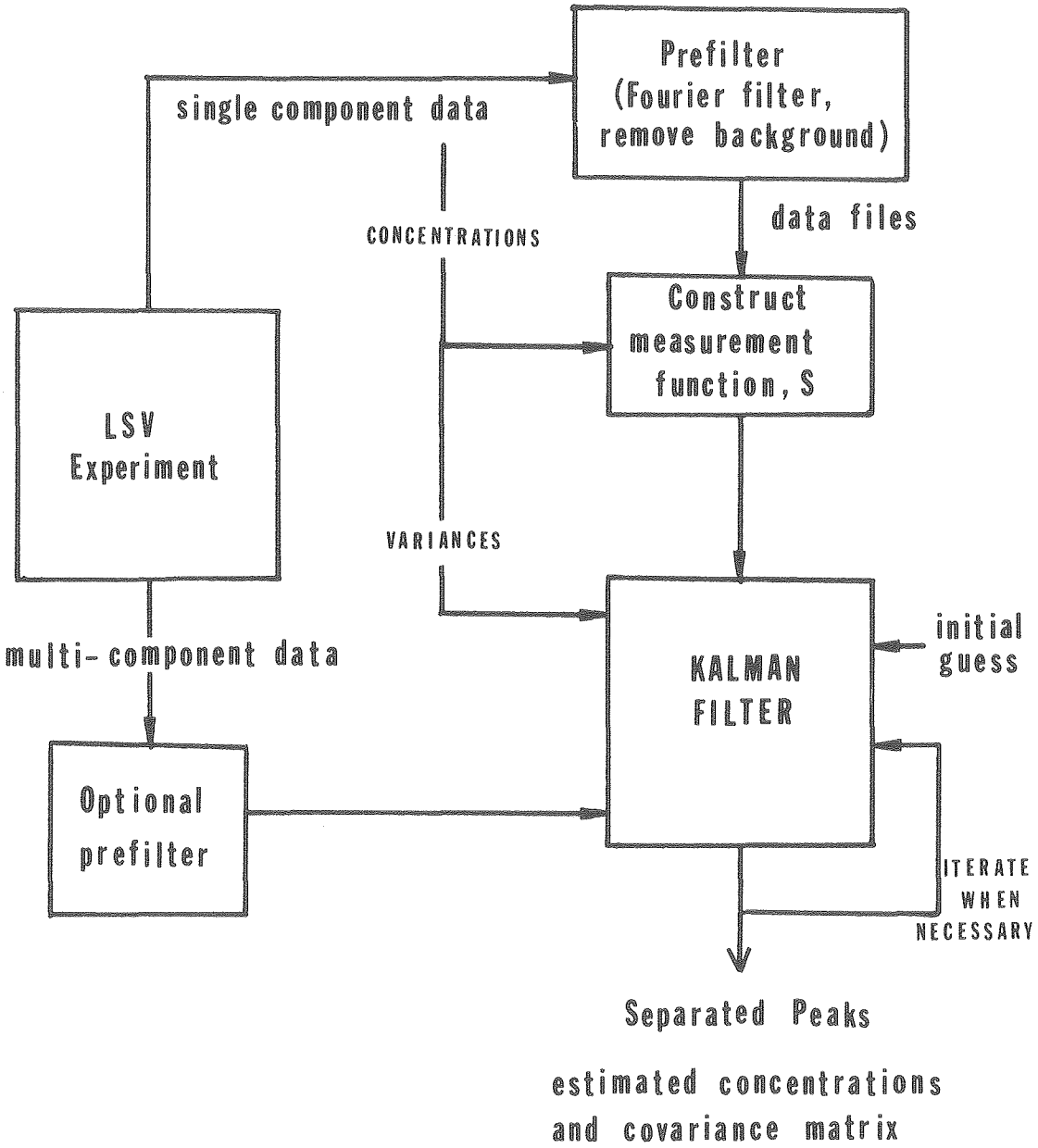
Prefilter
(Fourier filter,
remove background)
single component data
CONCENTRATIONS
data files
Construct
measurement
function, S
LSV
Experiment
VARIANCES
multi-component data
KALMAN
FILTER
initial
guess
Optional
prefilter
ITERATE
WHEN
NECESSARY
Separated Peaks
estimated concentrations
and covariance matrix
XBL 811-7550

Figure 2

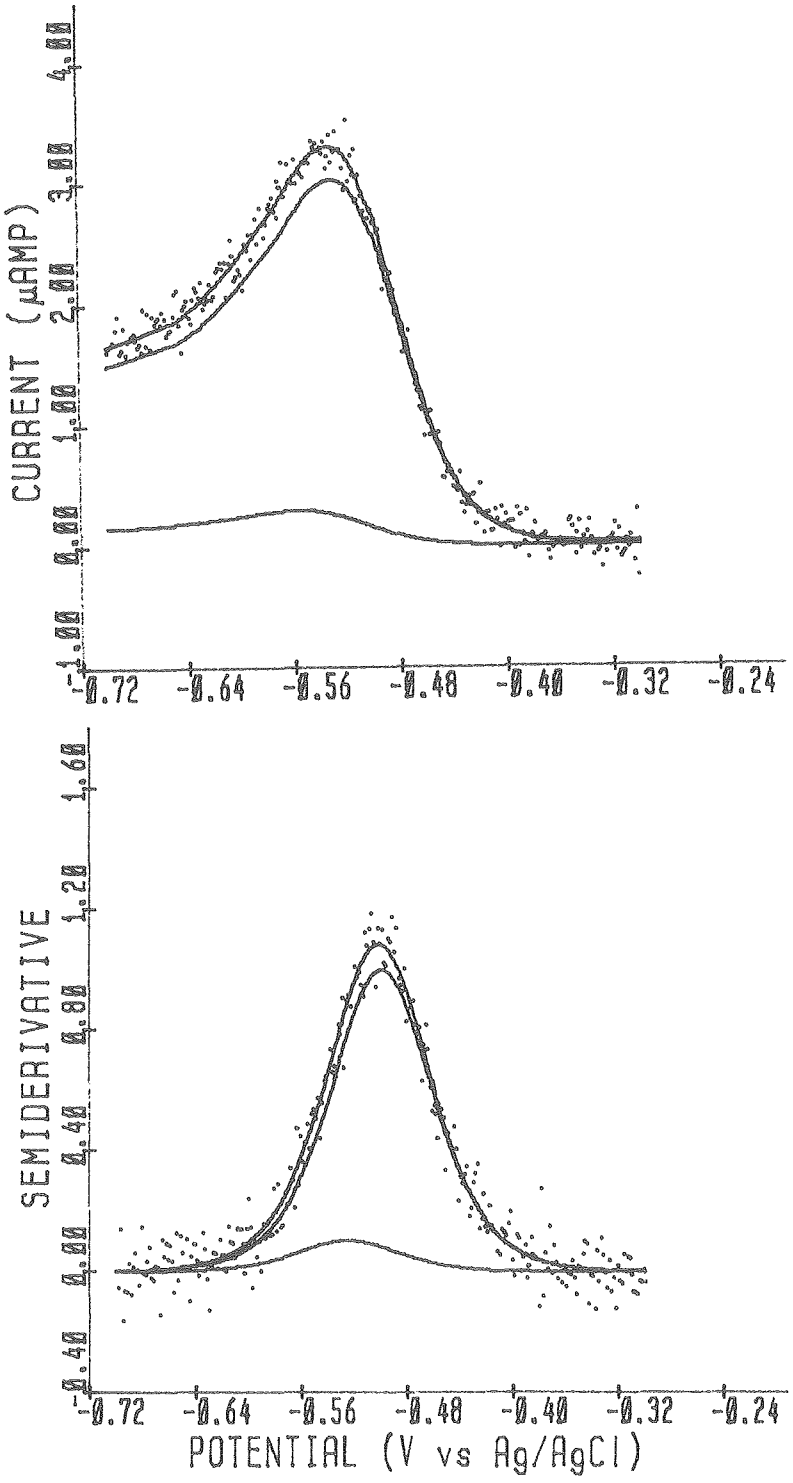
CURRENT (μAMP)
4.00
3.00
2.00
1.00
0.00
-1.00
-0.72
-0.64
-0.56
-0.48
-0.40
-0.32
-0.24
SEMIDERIVATIVE
1.60
1.20
0.80
0.40
0.00
-0.40
-0.72
-0.64
-0.56
-0.48
-0.40
-0.32
-0.24
POTENTIAL (V vs Ag/AgCl)
XBL 811-7551

Figure 3.

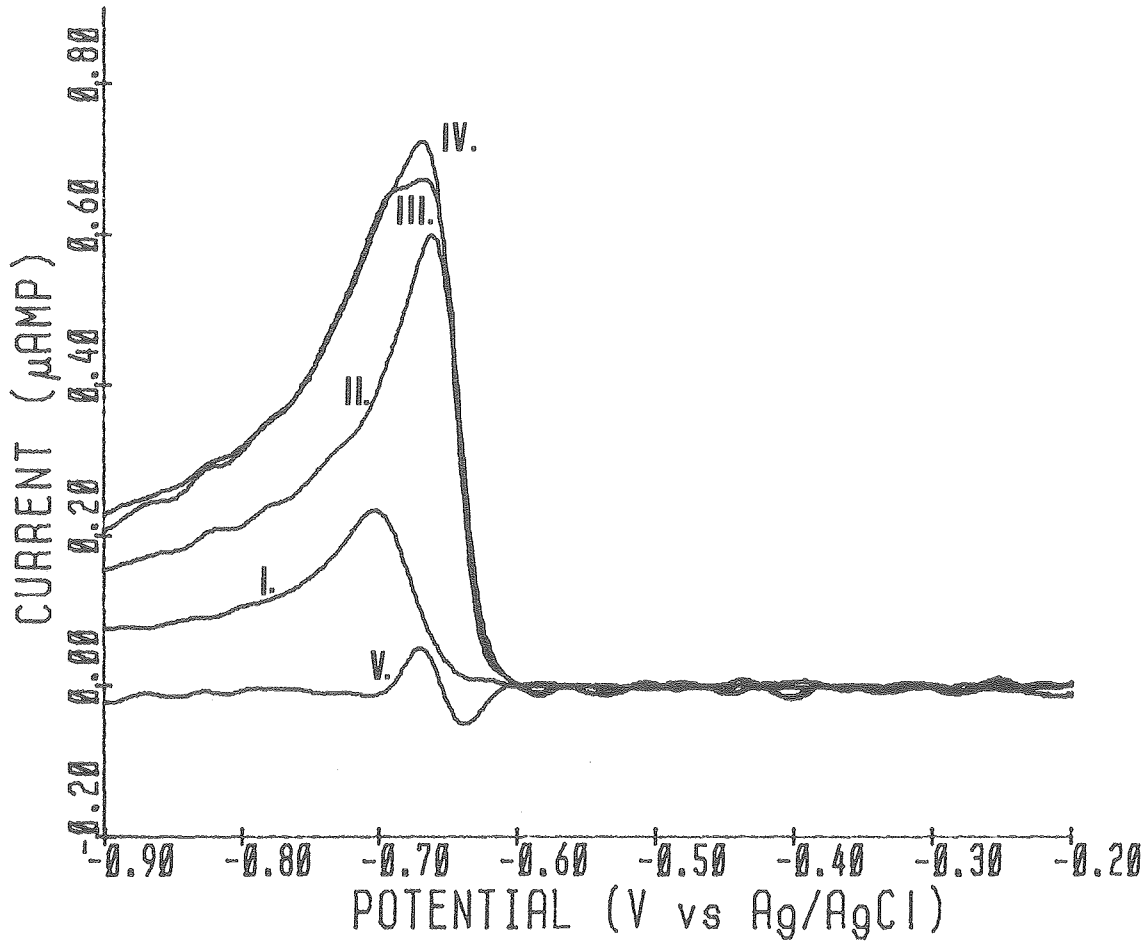

XBL 811-7552

Figure 4.

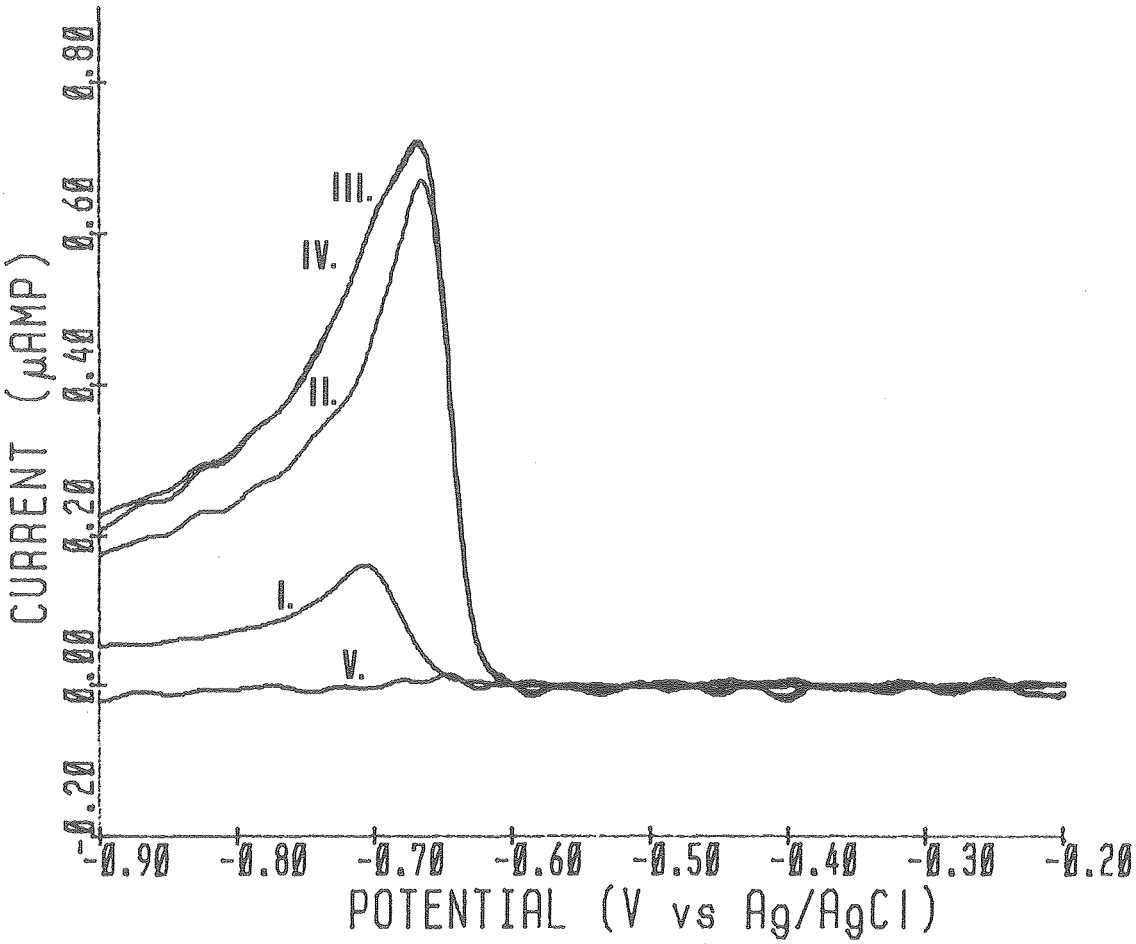

XBL 811-7553

Figure 5.

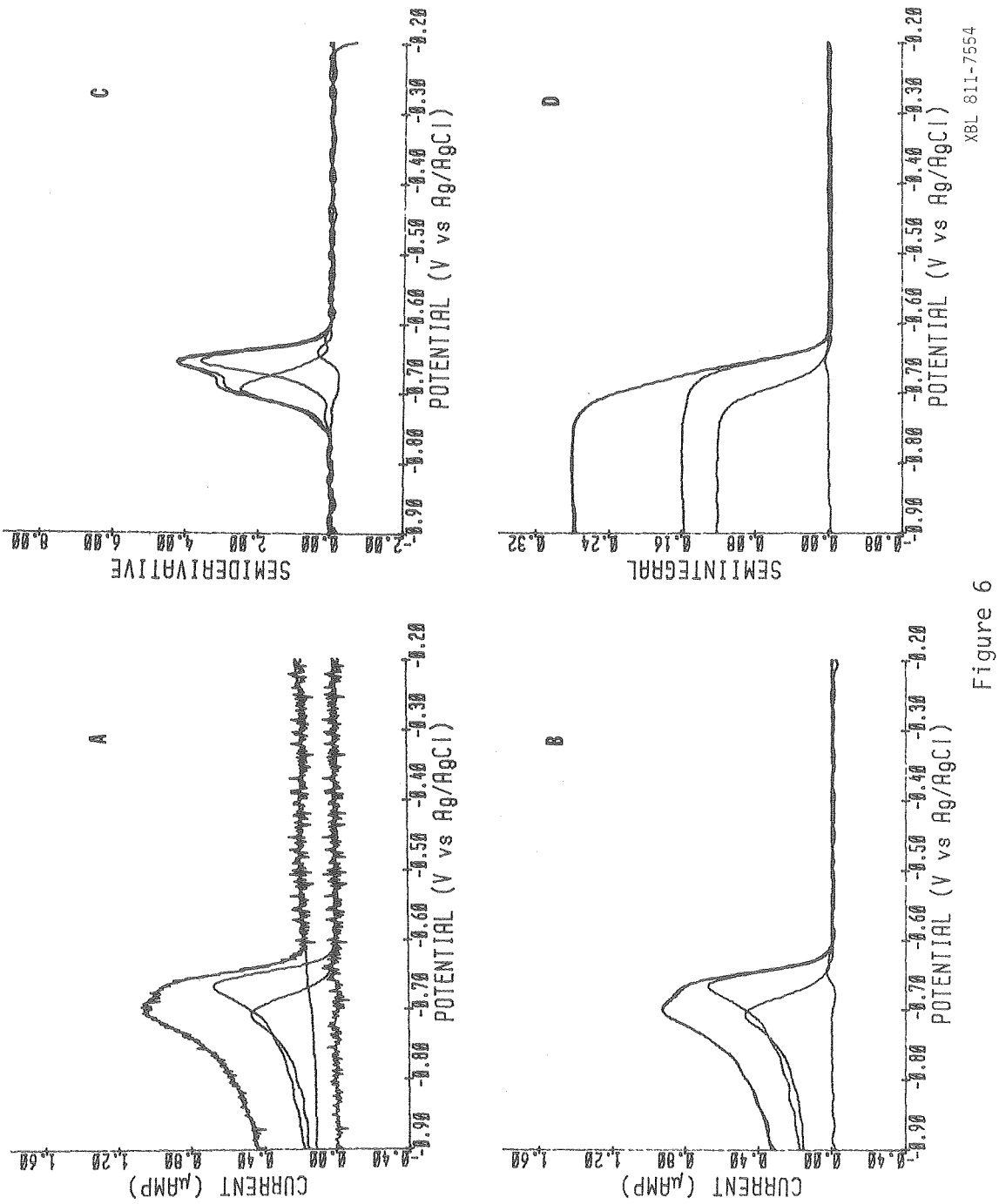
A
B
C
D
CURRENT (μAMP)
SEMIDERIVATIVE
SEMIINTEGRAL
POTENTIAL (V vs Ag/AgCl)
XBL 811-7554

Figure 6

Table I Summary of the Kalman Filter Equations for Discrete Time Measurements

Defining Equations:

System Model	$\underline{X}(k) = \underline{\underline{H}}(k,k-1)\cdot\underline{X}(k) + \underline{\underline{G}}(k)\cdot\underline{\omega}(k)$
Measurement Model	$\underline{Z}(k) = \underline{\underline{S}}(k)\cdot\underline{X}(k) + \underline{\nu}(k)$
Initial Conditions	$E[\underline{X}(0)] = \overline{\underline{X}}$
	$E[(\underline{X}(0)-\overline{\underline{X}})(\underline{X}(0)-\overline{\underline{X}})] = \underline{\underline{P}}$
Noise Assumptions	$\underline{\omega}(k) \equiv N(\underline{0},\underline{\underline{Q}}_k)$
	$\underline{\nu}(k) \equiv N(\underline{0},\underline{\underline{R}}_k)$
	$E[\underline{\omega}(k)\cdot\underline{\nu}(j)] = 0$ for all k,j

Algorithm Equations:

State Estimate Extrapolation	$\underline{X}(k\|k-1) = \underline{\underline{H}}(k,k-1)\cdot\underline{X}(k-1\|k-1)$
Error Covariance Extrapolation	$\underline{\underline{P}}(k\|k-1) = \underline{\underline{H}}\cdot\underline{\underline{P}}(k-1\|k-1)\cdot\underline{\underline{H}}^T + \underline{\underline{Q}}(k)$
Kalman Gain Equation	$\underline{\underline{K}}(k) = \underline{\underline{P}}(k\|k-1)\cdot\underline{\underline{S}}^T(k)\cdot[\underline{\underline{S}}\cdot\underline{\underline{P}}(k\|k-1)\cdot\underline{\underline{S}}^T + \underline{\underline{R}}]^{-1}$
State Estimate Update	$\underline{X}(k\|k) = \underline{X}(k\|k-1) + \underline{\underline{K}}(k)\cdot[\underline{Z}(k) - \underline{\underline{S}}\cdot\underline{X}(k\|k-1)]$
Error Covariance Update	$\underline{\underline{P}}(k\|k) = [\underline{\underline{I}} - \underline{\underline{K}}(k)\cdot\underline{\underline{S}}(k)]\cdot\underline{\underline{P}}(k\|k-1)$

Where

$\underline{X}(k)$ = the vector of state variables of length N at time k

$\underline{Z}(k)$ = the vector of measureables of length M at time k

$\underline{\omega}(k)$ = the vector of model noise of length L at time k

$\underline{\nu}(k)$ = the vector of measurement noise of length M at time k

$\underline{\underline{H}}(k,k-1)$ = the state transition matrix (N by N) between times k-1 and k

$\underline{\underline{S}}(k)$ = the measurement function matrix (M by N) at time k

$\underline{\underline{G}}(k)$ = the model noise matrix (N by L) at time k

$\underline{\underline{P}}(k)$ = the state covariance matrix (N by N) at time k

$\underline{\underline{K}}(k)$ = the gain or weight matrix (N by M) at time k

and where the notation

$A(k|j) \equiv$ the most probable value of A at time k conditioned on information from times upto and including j

$E[A] \equiv$ the expectation value of A

$N(A,B) \equiv$ a noise process with a mean value of A and a variance of B

$A^T \equiv$ the transpose of the matrix A

Table II. - The Kalman Filter Equations for the Analysis of Multi-component Voltammograms

Defining Equations:	
System Model	$\underline{X}(k) = \underline{\underline{I}} \cdot \underline{X}(k-1)$
Measurement Model	$Z(k) = \underline{S}^T(k) \cdot \underline{X}(k) + \nu(k)$
Initial Conditions	$\underline{X}_0$
	$\underline{\underline{P}}_0 = \underline{\underline{I}} \cdot \sigma_z^2$
Noise Assumptions	$\omega(k) \simeq 0$
	$\nu(k) \simeq N(\underline{0}, \sigma_z^2)$
Algorithm Equations:	
State Estimate Extrapolation	$\underline{X}(k\|k-1) = \underline{X}(k-1\|k-1)$
Error Covariance Extrapolation	$\underline{\underline{P}}(k\|k-1) = \underline{\underline{P}}(k-1\|k-1)$
Kalman Gain Equation	$\underline{K}(k) = \underline{\underline{P}}(k\|k-1) \cdot \underline{S}^T(k) \cdot [\underline{S} \cdot \underline{\underline{P}} \cdot \underline{S}^T + \sigma_z^2]$
State Estimate Update	$\underline{X}(k\|k) = \underline{X}(k-1\|k-1) + \underline{K} \cdot [Z - \underline{S}^T \cdot \underline{X}]$
Error Covariance Update	$\underline{\underline{P}}(k\|k) = [\underline{\underline{I}} - \underline{K} \cdot \underline{S}] \cdot \underline{\underline{P}}(k\|k)$

Table III. - Comparison of Synthetic LSV and SDV Results for a Two Component System

	Semiderivative Data				Linear Sweep Data			
FILE	E9	E10	E14	E15	A9	A10	A14	A15
ΔV[a]	25	25	10	10	25	25	10	10
PK HT[b]	1:1	1:1/10	1:1	1:1/10	1:1	1:1/10	1:1	1:1/10
S/N[c]	5.0	5.0	5.0	5.0	10.0	10.0	10.0	10.0
X(1)[d]	0.999	0.999	0.997	0.995	1.004	1.002	1.004	1.001
X(2)	1.003	0.105	1.001	0.092	0.998	0.100	0.999	0.100
P(1,1)[e]	2.0E-5	2.3E-5	3.0E-5	4.5E-5	4.3E-7	2.5E-5	2.4E-6	4.4E-5
P(1,2)	-7.8E-6	-1.7E-5	-1.1E-5	-3.2E-5	-4.1E-7	-2.2E-5	-2.3E-6	-4.2E-5
P(2,2)	2.0E-5	2.6E-5	3.0E-5	4.8E-5	4.6E-7	2.6E-5	2.4E-6	4.5E-5
VAR[f]	2.1E-2	2.1E-2	2.1E-2	2.1E-2	2.9E-2	9.1E-3	3.0E-2	9.3E-3
CD[f]	0.9901	0.9703	0.9981	0.9711	0.9975	0.9975	0.9974	0.9974
$\%e_1$[f]	0.1	0.1	0.3	0.5	0.4	0.2	0.4	0.1
$\%e_2$	0.3	5.0	0.1	8.0	0.2	0.0	0.1	0.0

a Difference in peak potentials of the two components (in mV)

b Ratio of peak heights of the two components

c Signal to noise ratio

d Estimated peak heights for the two components

e Estimated covariance matrix; $P(1,2) \equiv P(2,1)$

f Four measures of the fit: the variance of the fit, the coefficient of determination of the fit and the percent error in each component

Table IV. - Separation of Synthetic LSV Peaks of Equal Heights

	S/N = 100.				S/N = 10.			
$\Delta E_{1/2}$ [a]	$\%e_1$ [b]	$\%e_2$	VAR[c]	CD[d]	$\%e_1$	$\%e_2$	VAR	CD
50	0.00	0.00	4.1E-8	1.000	0.5	0.3	2.6E-2	0.9976
25	0.00	0.00	3.9E-8	1.000	0.4	0.2	2.9E-2	0.9975
10	0.00	0.00	5.0E-8	1.000	0.4	0.1	3.1E-2	0.9974
5	0.00	0.00	4.4E-8	1.000	0.1	0.4	3.1E-2	0.9974
2.5	0.00	0.01	4.0E-8	1.000	0.6	0.9	3.1E-2	0.9974

[a] Separation of peak potentials in mV

[b] Percent error found in each component

[c] Variance of the fit

[d] Coefficient of determination of the fit

Table V. - Detection of Peak Shifts Between Single Component and Multi-component Voltammograms

Peak Shift (mV)	$\%e_1$	$\%e_2$	VAR	CD	
+10.0	23.	21.	7.5E-3	0.9993	Shift increased
+ 5.0	10.	9.	1.9E-3	0.9998	apparent
+ 2.5	5.	4.	5.5E-4	0.9999	overlap
0.0	0.0	0.0	4.1E-8	1.000	
- 2.5	4.	4.	5.2E-4	1.000	Shift decreased
- 5.0	9.	8.	1.9E-3	0.9998	apparent
-10.0	16.	15.	7.3E-3	0.9993	overlap

Table VI. - The Effect of the Initial Guess on a Strongly Overlapped Three Component System

Guess	$\%e_1$	$\%e_2$	$\%e_3$	VAR	CD
True peak height ratio: 1:1:1					S/N = 100.
1.0:0.0:1.0	+4.3	-8.5	+4.4	9.0E-5	1.000
1.0:0.5:1.0	+2.2	-4.2	+2.2	2.8E-5	1.000
1.0:1.0:1.0	0.00	0.00	0.00	1.1E-7	1.000
True peak height ratio: $1:{}^1/_{10}:1$					S/N = 100.
1.0:0.0:1.0	+0.4	-8.4	+0.4	9.7E-7	1.000
1.0:0.5:1.0	-1.8	+34.	-1.8	1.4E-5	1.000
1.0:0.1:1.0	0.0	+0.1	0.0	6.6E-8	1.000
True peak height ratio: 1:1:1					S/N = 10.
1.0:0.0:1.0	+11.	-21.	+10.	6.0E-2	0.9975
1.0:0.5:1.0	+8.5	-16.	+7.8	6.0E-2	0.9974
1.0:1.0:1.0	+5.0	-9.0	+3.4	5.8E-2	0.9981
True peak height ratio: $1:{}^1/_{10}:1$					S/N = 10.
1.0:0.0:1.0	+4.0	-60.	+1.9	2.8E-2	0.9981
1.0:0.5:1.0	-11.	+240.	-15.	2.8E-2	0.9981
1.0:0.1:1.0	+0.9	+1.8	-1.4	2.8E-2	0.9981

Table VII. - The Effect of Changes in Peak Width Between Single Component and Multi-component Voltammograms

Conditions: 10 mV peak potential separation; peak height ratio of 1:10; peak width changes in larger peak only.

File	SC FWHM[a]	MC FWHM[b]	ΔFWHM	$\%e_1$	$\%e_2$	VAR	CD
E25	0.030	0.050	0.020	37.	600.	2.3E-2	0.9675
E26	0.045	0.050	0.005	5.6	200.	2.2E-3	0.9969
E27	0.050	0.050	0.000	1.5	15.	1.2E-5	1.000
E28	0.055	0.050	0.005	5.6	7.2	2.2E-3	0.9969
E29	0.060	0.050	0.010	15.	67.	7.8E-3	0.9890
E30	0.070	0.050	0.020	39.	370.	2.2E-2	0.9691

[a] Peak width at half maximum in the single component voltammogram

[b] Peak width at half maximum in the multi-component voltammogram

Table VIII. - Results for the Cadmium/Indium Systems with Allowed Peak Shifts of ±5 mV

Cadmium				Indium					
Conc[a]	PK HT[b]	PK HT_e[c]	%e	Conc	PK HT	PK HT_e	%e	VAR	CD
8.36	0.747	0.787	5.4	0.00	0.002	-0.032		1.0E-4	0.9995
8.36	0.747	0.783	4.8	1.62	0.187	0.193	3.4	1.4E-4	0.9995
8.36	0.747	0.761	1.9	3.24	0.372	0.411	1.0	1.9E-4	0.9996
8.36	0.747	0.758	1.4	4.85	0.550	0.577	5.0	2.6E-4	0.9995
8.36	0.747	0.748	0.2	6.47	0.740	0.778	5.1	4.4E-4	0.9994
8.36	0.747	0.818	9.5	8.09	0.924	0.889	-3.8	2.7E-4	0.9997
0.00	0.002	0.001		5.88	0.670	0.675	0.7	3.7E-5	0.9998
1.67	0.150	0.161	6.5	5.88	0.670	0.664	-0.9	5.3E-5	0.9998
3.34	0.300	0.292	-2.9	5.88	0.670	0.655	-2.2	7.0E-5	0.9997
5.01	0.448	0.474	5.8	5.88	0.670	0.667	-0.4	1.1E-4	0.9997
6.68	0.597	0.583	-2.3	5.88	0.670	0.661	-1.4	1.4E-4	0.9997
8.36	0.747	0.745	-0.4	5.88	0.670	0.662	-1.1	1.8E-4	0.9997

Peak Shifts:

Cd(II) -4 mV from -0.702 to -0.706 V vs. Ag/AgCl

In(III) -3 mV from -0.662 to -0.665 V vs Ag/AgCl

[a] Concentrations in 10^{-5} M

[b] Theoretical peak heights based on single component standard addition curves

[c] Kalman filter estimate of peak heights

Table IX. - Results for the Three Component Cd(II)/In(III)/Pb(II) System with ±5 mV Peak Shifts Allowed

Cadmium				Indium				Lead					
Conc[a]	PK HT[b]	PK HT_e[c]	%e	Conc	PK HT	PK HT_e	%e	Conc	PK HT	PK HT_e	%e	VAR	CD
0.00	0.002	0.004		8.09	0.924	0.915	0.9	7.86	0.814	0.852	4.7	3.4E-4	0.9995
1.67	0.150	0.162	8.0	8.09	0.924	0.887	4.0	7.86	0.814	0.846	3.9	3.0E-4	0.9991
3.34	0.300	0.311	3.7	8.09	0.924	0.875	5.3	7.86	0.814	0.841	3.3	3.0E-4	0.9992
5.01	0.448	0.455	1.6	8.09	0.924	0.883	4.4	7.86	0.814	0.848	4.2	3.4E-4	0.9992
6.68	0.597	0.603	1.0	8.09	0.924	0.891	3.6	7.86	0.814	0.828	1.7	3.6E-4	0.9993
8.36	0.747	0.780	4.4	8.09	0.924	0.903	2.3	7.86	0.814	0.846	3.9	2.8E-4	0.9996

Peak Shifts:

Cd(II) -1.4 mV from -0.702 to -0.703

In(III) -1.4 mV from -0.662 to -0.663

Pb(II) -4.1 mV from -0.498 to -0.502

[a] Concentrations in 10^{-5} M

[b] Theoretical peak heights based on single component standard addition curves

[c] Kalman Filter estimate of the peak heights